Polarization observables in $\gamma N \to K \overline{K} N$

W. Roberts*

Department of Physics, Old Dominion University, Norfolk, Virginia 23529, USA, and
Continuous Electron Beam Accelerator Facility 12000 Jefferson Avenue, Newport News, Virginia 23606, USA

Some of the rich structure of the polarization observables recently developed for processes like $\gamma N \to \pi \pi N$ and $\gamma N \to K \overline{K} N$ are explored within the framework of a specific model for the latter process. Emphasis is placed on observables that may be accessible at existing facilities in the near future. The sensitivity of the observables to the details of the model indicate that they will be a very useful tool in differentiating among models used to describe reactions like these. Within the framework of a model for $\gamma N \to K \overline{K} N$, the sensitivity of the observables to the coupling constants of the ϕ, to the properties of the $\Lambda(1405)$, and to the existence of the Θ^+ is examined.

PACS number(s): 13.60.Rj, 13.60.Le, 13.88.+e

I. INTRODUCTION AND MOTIVATION

In a recent article [1], sets of polarization observables for the processes $\pi N \to \pi \pi N$ and $\gamma N \to \pi \pi N$ were introduced. In this paper, some of these observables are examined in the context of a specific model for the process $\gamma N \to K \overline{K} N$. Four different facets of these polarization observables are explored. First, the expected sizes of these observables are examined. Obviously, if these observables are too small, they may not be of interest to experimentalists. It turns out that some of the observables, including some that can be obtained in the near future at present facilities, can be quite large.

The sensitivity of the observables to the details of the underlying dynamics is also explored, thus illustrating how they will be useful in helping to pin down parameters in any model used to describe such processes. In addition, since these observables are fivefold differential observables, various ways of presenting them are examined, noting that the same observable can appear very different depending on what is chosen as the independent kinematic variables. Finally, the potential of these observables in the hunt for resonances is examined in model calculations with the Θ^+ included, and with it excluded. The sensitivity to the parity of the Θ^+ is also examined, assuming that it has spin 1/2.

The focus is on the 16 observables that may be readily measured at present facilities like Jefferson Lab, Bonn, and Graal, for example. The availability of linearly or circularly polarized beams at these facilities, along with advances in the technology for the production of polarized targets, means that a number of these observables can, in principle, be measured with high precision. Indeed, first measurements of $I^\odot$, the beam asymmetry that arises with circularly polarized photons, in $\gamma p \to p \pi^+ \pi^-$ indicate that even the smaller asymmetries can be measured with good precision [2]. Triple-polarization observables can be measured from the self-analyzing decays of hyperons produced in processes like $\gamma N \to \pi K Y$. However, such observables will be more difficult to measure for processes like $\gamma N \to \pi \pi N$, as none of the present facilities are equipped to measure recoil polarizations.

It must be emphasized here that the focus of this paper is the polarization observables and what they can convey about the underlying dynamics of the process being investigated, *not* the particular model that we are using to illustrate the power of these observables. Models of this sort can always be criticized for lacking such and such an effect, for treating this or that state in a questionable way, etc. The model, in this case, is simply a vehicle for showing the potential power that is inherent in the polarization observables.

With that said, however, it must be pointed out that the model used [3] is, as far as can be ascertained, the only one that provided a critical assessment of pentaquark signals seen in two photoproduction experiments that used proton targets [4]. Recently, the CLAS collaboration at Jefferson Laboratory presented results in which the upper limit for the production cross section of the pentaquark was "a few nanobarns" [5]. It therefore appears that the analysis in Ref. [3] was largely correct, as such a cross section is very similar to the model predictions obtained in Ref. [3] for a state with $J^P = 1/2^+$. If the state does exist and has such a small production cross section, polarization observables will be crucial for the extraction of any signal.

The rest of this paper is organized as follows. In the next section, the observables are briefly discussed, while Sec. III provides a discussion of the model that is used to calculate the observables. Much of the discussion of the model has been presented in Ref. [3], but is repeated here for the sake of completeness. In Sec. IV, the results obtained are presented; the sensitivity of a few of the observables to (a) the coupling constants of the ϕ meson; (b) the $\Lambda(1405)$, and (c) the presence of the Θ^+, including its parity, are examined. Section V presents conclusions and an outlook.

II. OBSERVABLES

The reaction rate I, for the process $\gamma N \to K \overline{K} N$, can be written

$$
\begin{aligned}
\rho_f I = I_0 \big\{ & \big(1 + \vec{\Lambda}_i \cdot \vec{P} + \vec{\sigma} \cdot \vec{P}' + \Lambda_i^\alpha \sigma^{\beta'} \mathcal{O}_{\alpha \beta'} \big) \\
& + \delta_\odot \big(I^\odot + \vec{\Lambda}_i \cdot \vec{P}^\odot + \vec{\sigma} \cdot \vec{P}^{\odot'} + \Lambda_i^\alpha \sigma^{\beta'} \mathcal{O}_{\alpha \beta'}^\odot \big) \\
& + \delta_\ell \big[\sin 2\beta \big(I^s + \vec{\Lambda}_i \cdot \vec{P}^s + \vec{\sigma} \cdot \vec{P}^{s'} + \Lambda_i^\alpha \sigma^{\beta'} \mathcal{O}_{\alpha \beta'}^s \big) \\
& + \cos 2\beta \big(I^c + \vec{\Lambda}_i \cdot \vec{P}^c + \vec{\sigma} \cdot \vec{P}^{c'} + \Lambda_i^\alpha \sigma^{\beta'} \mathcal{O}_{\alpha \beta'}^c \big) \big] \big\},
\end{aligned} \quad (1)
$$

*On leave at the Office of Nuclear Physics, Department of Energy, 19901 Germantown Road, Germantown, Maryland 20874, USA.

035215-1

where $\vec{P}$ represents the polarization asymmetry that arises if the target nucleon has polarization $\vec{\Lambda}_i$, $\rho_f = \frac{1}{2}(1 + \vec{\sigma} \cdot \vec{P}')$ is the density matrix of the recoiling nucleon, and $\mathcal{O}_{\alpha\beta'}$ is the observable if both the target and the recoil polarization are measured. The primes indicate that the recoil observables are measured with respect to a set of axes x', y', z', in which z' is along the direction of motion of the recoiling nucleon, and $y' = y$. $\delta_{\odot}$ is the degree of circular polarization in the photon beam, while δ_{ℓ} is the degree of linear polarization, with the direction of polarization at an angle β to the x axis.

Of these 63 polarization observables (I_0 is proportional to the unpolarized differential cross section), 48 require detection of the polarization of the recoil nucleon. Since none of the present facilities are equipped for such measurements, little attention is devoted to such observables at this time. Note, however, that such observables will be essential for unambiguously extracting the helicity or transversity amplitudes that describe this process. A more detailed discussion of the formalism for these observables, including their definitions in terms of helicity and transversity amplitudes, the quadratic identities and inequalities that they satisfy, and the classes of measurements needed for extraction of the helicity or transversity amplitudes, is presented in [1].

III. MODEL

The framework in which the process $\gamma N \to N K \overline{K}$ is treated is the phenomenological Lagrangian approach. In this approach, all particles are treated as pointlike. Their structure is accounted for by inclusion of phenomenological form factors, which are discussed in a later subsection. What follows is a slightly modified version of the discussion in [3]. In this paper, the spin of the Θ^+ in restricted to 1/2 and its isospin to zero; its couplings to K^* mesons are also neglected.

A. Ground-state baryons

The first ingredients of the model are the Lagrangian terms needed for the electromagnetic vertices of pseudoscalar mesons and ground-state baryons. Nucleons are treated as isospin doublets with $N = \binom{p}{n}$. Kaons are also treated as isospin doublets $\left[K = \binom{K^+}{K^0} \right]$. π and Σ are treated as isotriplets.

In what should be a transparent notation, the electromagnetic part of the Lagrangian is (with the Θ^+ omitted for the time being)

$$
\begin{aligned}
\mathcal{L}_1 = &\overline{N}\left[-\frac{e}{2}(1+\tau_3)\gamma_\mu A^\mu + \frac{e}{4M_N}\left(k_s^N + \tau_3 k_v^N\right)\gamma_\mu \gamma_\nu F^{\mu\nu} \right] N \\
&+ \overline{\Sigma}\left[-\frac{e}{2}(1+T_3)\gamma_\mu A^\mu + \frac{e}{4M_\Sigma}\left(k_s^\Sigma + \tau_3 k_v^\Sigma\right)\gamma_\mu \gamma_\nu F^{\mu\nu} \right]\Sigma \\
&+ \overline{\Lambda}\frac{e}{4M_\Lambda}\mu_\Lambda \gamma_\mu \gamma_\nu F^{\mu\nu}\Lambda + \overline{\Sigma^0}\frac{e}{2(M_\Sigma^0 + M_\Lambda)}\mu_{\Sigma\Lambda}\gamma_\mu \gamma_\nu F^{\mu\nu}\Lambda \\
&- \frac{e}{2}[K^\dagger(1+\tau_3)(\partial_\mu K) - (\partial_\mu K^\dagger)(1+\tau_3)K]A^\mu + \text{H.c.},
\end{aligned}
\tag{2}
$$

where $\mu_{\Sigma\Lambda}$ is the $\Sigma^0 \to \Lambda$ transition magnetic moment, μ_Λ is the magnetic moment of the Λ, k_s^N and k_v^N describe the anomalous magnetic moments of the nucleon doublet, and the $k_{s,v}^\Sigma$ are the corresponding quantities for the Σ isotriplet. T_3 is the isospin operator for the isotriplet.

The coupling of pseudoscalar mesons to ground-state baryons is described by the Lagrangian

$$
\begin{aligned}
\mathcal{L}_2 = &\frac{g_{NN\pi}}{2M_N}\overline{N}\gamma_\mu \gamma_5 (\partial^\mu \pi \cdot \tau)N + \frac{g_{N\Lambda K}}{M_N + M_\Lambda}\overline{N}\gamma_\mu \gamma_5(\partial^\mu K)\Lambda \\
&+ \frac{g_{N\Sigma K}}{M_N + M_\Sigma}\overline{N}\gamma_\mu \gamma_5 \Sigma \cdot \tau \partial^\mu K + \frac{g_{NN\eta}}{2M_N}\overline{N}\gamma_\mu \gamma_5 N(\partial^\mu \eta) \\
&- e\frac{g_{NN\pi}}{2M_N}\overline{N}\gamma_\mu \gamma_5 A^\mu \tau_3 \pi \cdot \tau N \\
&- e\frac{g_{N\Lambda K}}{M_N + M_\Lambda}\overline{N}\gamma_\mu \gamma_5 A^\mu \tau_3 K \Lambda \\
&- e\frac{g_{N\Sigma K}}{M_N + M_\Sigma}\overline{N}\gamma_\mu \gamma_5 \Sigma \cdot \tau A^\mu \tau_3 K + \text{H.c.}
\end{aligned}
\tag{3}
$$

In this expression, η is an isosinglet field representing the η meson. The last three terms of this Lagrangian are obtained by minimal substitution in the first three terms.

B. Vector mesons

The vector mesons that enter into the model are K^* and ϕ. The K^* is treated as a vector-isodoublet field K_μ, completely analogously to the K, while the ϕ is represented by a vector isosinglet field ϕ_μ. The Lagrangian in this sector is

$$
\begin{aligned}
\mathcal{L}_3 = &\overline{N}\left[G_v^\phi \gamma^\mu \phi_\mu + i\frac{G_t^\phi}{2M_N}\gamma^\mu \gamma^\nu (\partial_\nu \phi_\mu) \right]N \\
&+ \overline{N}\left[G_v^{K^*N\Lambda}\gamma^\mu K_\mu^* + i\frac{G_t^{K^*N\Lambda}}{M_N + M_\Lambda}\gamma^\mu \gamma^\nu (\partial_\nu K_\mu^*) \right]\Lambda \\
&+ \overline{N}\left(G_v^{K^*N\Sigma}\gamma^\mu \Sigma \cdot \tau K_\mu^* + i\frac{G_t^{K^*N\Sigma}}{M_N + M_\Sigma}\gamma^\mu \gamma^\nu \Sigma \cdot \tau \partial_\nu K_\mu^* \right) \\
&+ \epsilon^{\alpha\beta\mu\nu}\left[\frac{g_{\phi\pi\gamma}}{m_\pi}\phi_\alpha(\partial_\mu A_\beta)\partial_\nu \pi^0 + \frac{g_{\phi\eta\gamma}}{m_\eta}\phi_\alpha(\partial_\mu A_\beta)\partial_\nu \eta \right] \\
&+ \frac{g_{\phi KK}}{m_K}[K^\dagger(\partial^\mu K) - (\partial^\mu K^\dagger)K]\phi_\mu \\
&+ \frac{g_{K^*K\pi}}{m_K}[K^\dagger(\partial^\mu \pi \cdot \tau) - (\partial^\mu K^\dagger)\pi \cdot \tau]K_\mu^*.
\end{aligned}
\tag{4}
$$

C. Baryon resonances

There are a number of resonances that need to be taken into account in a calculation such as this. Since the experimental target is a nucleon, any of the nucleon or Δ resonances are expected to play a role. The contributions of such resonances are ignored in the results that follow, mainly because they have been found to be small. However, a more complete calculation should take such contributions into account. Among the hyperons, the scope is limited so that only the lowest few hyperon resonances are taken into account. In either case, no baryon with spin greater than 3/2 is considered. With the scope of the model limited in this way this, there are only a few Lagrangian terms that must be considered in this

TABLE I. Values of g_{YNK} for nonexotic hyperons appearing in the model.

Y(Mass)	J^P	Γ (MeV)	$\frac{\Gamma_{NK}}{\Gamma}$	g_{YNK}
$\Lambda(1520)$	$\frac{3}{2}^-$	16	0.45	15.2
$\Lambda(1600)$	$\frac{1}{2}^+$	150	0.2	1.05
$\Lambda(1670)$	$\frac{1}{2}^-$	35	0.25	0.32
$\Lambda(1690)$	$\frac{3}{2}^-$	60	0.25	5.53
$\Lambda(1800)$	$\frac{1}{2}^+$	300	0.35	0.86
$\Lambda(1810)$	$\frac{1}{2}^+$	150	0.35	0.71
$\Lambda(1890)$	$\frac{3}{2}^+$	100	0.3	1.09
$\Sigma(1580)$	$\frac{3}{2}^-$	15	0.45	1.95
$\Sigma(1620)$	$\frac{1}{2}^-$	80	0.22	0.52
$\Sigma(1660)$	$\frac{1}{2}^+$	100	0.2	0.67
$\Sigma(1670)$	$\frac{3}{2}^-$	60	0.1	3.88
$\Sigma(1750)$	$\frac{1}{2}^-$	90	0.26	0.44
$\Sigma(1880)$	$\frac{1}{2}^+$	80	0.06	0.19
$\Sigma(1940)$	$\frac{3}{2}^-$	220	0.13	3.19

sector. The nonexotic hyperons that are included are listed in Table I.

1. Spin 1/2

Lagrangian terms needed for spin-1/2 resonances are

$$
\begin{aligned}
\mathcal{L}_4 = {} & \overline{N}\frac{g_{\Sigma^*NK}^{(\frac{1}{2})}}{m_K}\gamma_\mu\gamma_5\Sigma^*\cdot\tau\partial^\mu K + \overline{N}\frac{g_{\Lambda^*NK}^{(\frac{1}{2})}}{m_K}\gamma_\mu\gamma_5(\partial^\mu K)\Lambda^* \\
& + \overline{N}\frac{g_{\Theta NK}^{(\frac{1}{2})}}{m_K}\gamma_\mu\gamma_5(\partial^\mu K)\Theta_+ \\
& + \overline{N}\frac{g_{\Sigma^*NK}^{(\frac{1}{2})}}{m_K}\gamma_\mu\Sigma^*\cdot\tau\partial^\mu K + \overline{N}\frac{g_{\Lambda^*NK}^{(\frac{1}{2})}}{m_K}\gamma_\mu(\partial^\mu K)\Lambda^* \\
& + \overline{N}\frac{g_{\Theta NK}^{(\frac{1}{2})}}{m_K}\gamma_\mu(\partial^\mu K)\Theta_- + \text{H.c.,}
\end{aligned} \tag{5}
$$

where $\Theta_\pm$ is the field for Θ^+ with $J^P = 1/2^\pm$. The first three terms of this Lagrangian correspond to states with $J^P = 1/2^+$, while the last three terms are for $J^P = 1/2^-$. In addition, the Θ^+ part of the Lagrangian written above assumes that the state is an isosinglet.

2. Spin 3/2

The Lagrangian terms for spin-3/2 resonances are

$$
\begin{aligned}
\mathcal{L}_6 = {} & \overline{N}\frac{g_{\Sigma^*NK}^{(\frac{3}{2})}}{m_K}\Sigma_\mu^*\cdot\tau\partial^\mu K + \overline{N}\frac{g_{\Lambda^*NK}^{(\frac{3}{2})}}{m_K}(\partial^\mu K)\Lambda_\mu^* \\
& + \overline{N}\frac{g_{\Sigma^*NK}^{(\frac{3}{2})}}{m_K}\gamma_5\Sigma_\mu^*\cdot\tau\partial^\mu K \\
& + \overline{N}\frac{g_{\Lambda^*NK}^{(\frac{3}{2})}}{m_K}\gamma_5(\partial^\mu K)\Lambda_\mu^* + \text{H.c.,}
\end{aligned} \tag{6}
$$

TABLE II. Values of $g_{BB'M}$ obtained with the Goldberger-Treimann relations.

Coupling	f_M (GeV)	$\left(\frac{G_A}{G_V}\right)_{B \to B'}$	$g_{BB'M}$
$g_{\pi NN\pi}$	$\frac{0.13}{\sqrt{2}}$	1.22	12.8
$g_{N\Sigma K}$	$\frac{0.16}{\sqrt{2}}$	0.34	3.2
$g_{N\Lambda K}$	$\frac{0.16}{\sqrt{2}}$	-0.718	-6.51
$g_{NN\eta}$	$\approx 1.2 f_\pi$	1.22	10.37

where the μ indices on the Λ and Σ fields indicate that they are vector-spinor, spin-3/2 fields. In this calculation, the Rarita-Schwinger version of such fields is used. The first two terms are for resonances with positive parity, while the last two are for resonances with negative parity.

D. Coupling Constants

To evaluate the coupling constants of the ground-state baryons to pseudoscalar mesons, the extended Goldberger-Treimann relations are used. For the coupling of the baryons B and B' to the pseudoscalar M, the relation is

$$
g_{BB'M} = \left(\frac{G_A}{G_V}\right)_{B \to B'}\frac{M_B + M_{B'}}{2 f_M}, \tag{7}
$$

where f_M is the meson decay constant for the pseudoscalar meson M. $\left(\frac{G_A}{G_V}\right)_{B \to B'}$ is obtained from the semileptonic decay of $B \to B'$ or $B' \to B$. The values of f_M, $\left(\frac{G_A}{G_V}\right)_{B \to B'}$ (taken from the *Review of Particle Physics* [6]) and $g_{BB'M}$ obtained from these relations are shown in Table II.

The decay width of a vector meson into two pseudoscalars is related to the corresponding coupling constant by

$$
\Gamma_{V \to P_1 P_2} = \frac{g_{V P_1 P_2}^2}{48\pi M_V^5}\lambda^{\frac{3}{2}}\left(M_V^2, M_{P_1}^2, M_{P_2}^2\right), \tag{8}
$$

where $\lambda(a, b, c)$ is the Källen function, with $\lambda(a, b, c) = a^2 + b^2 + c^2 - 2(ab + ac + bc)$. From the measured widths and branching fractions of the ϕ and K^* mesons, the values

$$
g_{\phi KK} = 4.3, \quad g_{K^*K\pi} = 5.6 \tag{9}
$$

are obtained. In a similar way, the width for the process $V \to P\gamma$ is

$$
\Gamma_{V \to P\gamma} = \frac{g_{V P\gamma}^2}{192\pi M_V^3}\lambda^{\frac{3}{2}}\left(M_V^2, M_P^2, 0\right), \tag{10}
$$

which leads to

$$
\begin{aligned}
g_{\phi\eta\gamma} &= 4.3, \quad g_{\phi\pi^0\gamma} = 0.055, \\
g_{K^{0*}K^0\gamma} &= 0.35, \quad g_{K^{+*}K^+\gamma} = 0.22.
\end{aligned} \tag{11}
$$

For a baryon B with $J^P = 1/2^+$, the width for the decay into a pseudoscalar meson P and a ground-state baryon B' is

$$
\begin{aligned}
\Gamma_{B \to B'P} = {} & \frac{g_{BB'P}^2}{16\pi M_B^3 M_P^2}(M_B + M_{B'})^2 \\
& \times [(M_B - M_{B'})^2 - M_P^2]\lambda^{\frac{1}{2}}\left(M_B^2, M_{B'}^2, M_P^2\right),
\end{aligned} \tag{12}
$$

while the corresponding width for a baryon with $J^P = 1/2^-$ is

$$\Gamma_{B \to B'P} = \frac{g_{BB'P}^2}{16\pi M_B^3 M_P^2} (M_B - M_{B'})^2$$
$$\times [(M_B + M_{B'})^2 - M_P^2] \lambda^{\frac{1}{2}} (M_B^2, M_{B'}^2, M_P^2). \quad (13)$$

For baryons with $J^P = 3/2^\pm$, the widths are

$$\Gamma_{B \to B'P} = \frac{g_{BB'P}^2}{192\pi M_B^5 M_P^2} [(M_B + M_{B'})^2 - M_P^2] \lambda^{\frac{3}{2}} (M_B^2, M_{B'}^2, M_P^2),$$
$$(14)$$
$$\Gamma_{B \to B'P} = \frac{g_{BB'P}^2}{192\pi M_B^5 M_P^2} \frac{\lambda^{\frac{5}{2}} (M_B^2, M_{B'}^2, M_P^2)}{[(M_B + M_{B'})^2 - M_P^2]},$$

where the first expression is for a positive-parity parent baryon. The nonexotic hyperons that are used in this calculation, along with their masses, total widths, spins, parities, and their NK branching fractions and coupling constants, obtained from Eqs. (12)–(14), are shown in Table I.

As mentioned above, the Θ pentaquarks are allowed to have $J^P = 1/2^\pm$. In [3], this state was also allowed to have $J^P = 3/2^\pm$, but the cross sections for production of such a state are much larger than the upper limits reported by the CLAS Collaboration [5]. The present discussion is therefore restricted to a Θ^+ with spin 1/2. The width of the Θ^+ is chosen to be 1 MeV, consistent with various analyses reported in the literature [7]. The values of the coupling constants obtained for the different parities of the Θ are $g_{\Theta NK}^{(\frac{1}{2})} = 0.27$ for positive parity and $g_{\Theta NK}^{(\frac{1}{2})} = 0.16$ for negative parity. These values are obtained assuming that the NK final state saturates the decays of the Θ^+.

There are a number of coupling constants for which little information is available. Perhaps the most important of these in terms of contributions to the cross sections are the couplings of the vector mesons K^* and ϕ, particularly those of the ϕ to the ground-state nucleons. The couplings of the two hyperon resonances that lie below the NK threshold, namely the $\Sigma(1385)$ and the $\Lambda(1405)$, are also not known with much certainty. In the discussion of the polarization observables, the effects of different values of the coupling constants of the ϕ, as well as those of the $\Lambda(1405)$, will be explored.

E. Diagrams

The diagrams included in this calculation are shown in Figs. 1 and 3. In these diagrams, solid lines represent baryons. If a solid line is unlabeled, it represents a nucleon. Dashed lines represent pseudoscalar mesons, and unlabeled dashed lines represent kaons. Wavy lines are photons, and dotted lines are vector mesons. Each diagram shown actually represents a
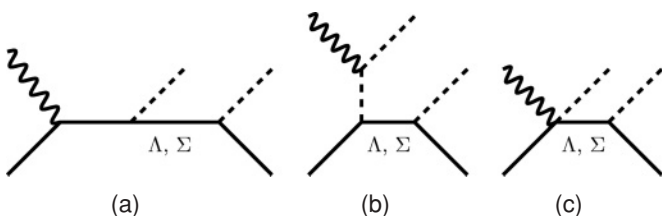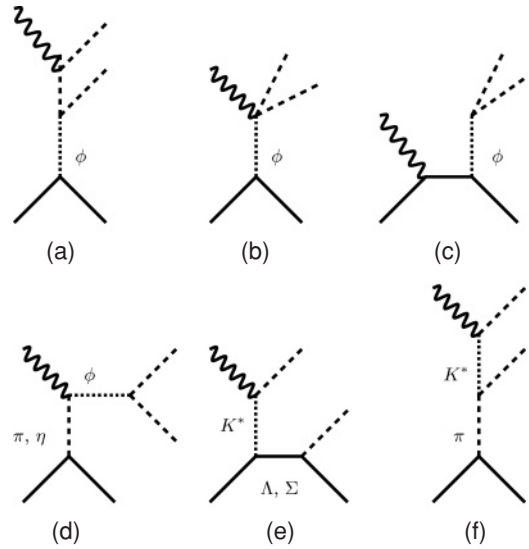

FIG. 2. Diagrams containing vector mesons. The dotted lines represent the vector mesons.

set of diagrams, as all allowed permutations of external meson and photon legs are taken into account.

A number of hyperon resonances are included in this calculation. These are listed in Table I. For each of the resonances, there is a corresponding set of diagrams of the kind shown in Fig. 3.

There are a number of contributions that have been omitted from this calculation. For instance, all but the ground-state nucleon and all of the Δ resonances are omitted. In fact, with the information that is available on how these states couple to final states with hidden strangeness, it was found that their contributions to the cross section are small. Couplings to higher moments of any of the hyperon resonances have also been neglected [Fig. 3(d)], as well as any contributions that would arise from electromagnetic transitions between excited hyperons and their ground states. In principle, there is no
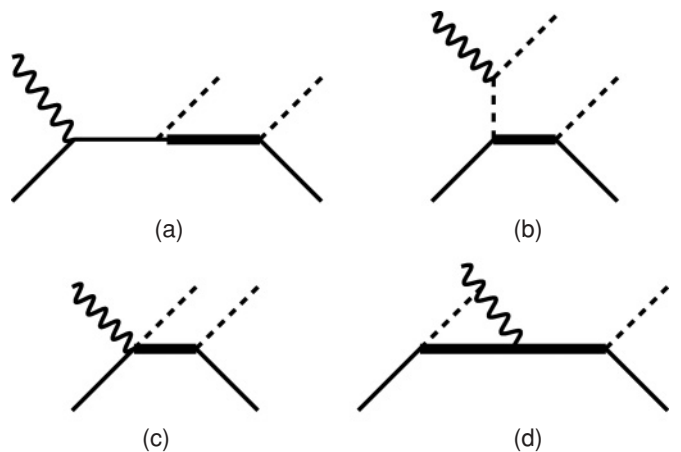

FIG. 1. "Born" diagrams: Solid unlabeled lines are nucleons; unlabeled dashed lines are kaons; and wavy lines are photons.

FIG. 3. Diagrams containing excited baryons. In (a)–(d), the thick solid lines may be either Λ^*, Σ^* or Θ, while the thin solid line is a nucleon. In diagram (d), the photon couples to the charge of the intermediate resonance: In this model, couplings to any higher electromagnetic moments of the resonance are neglected.

a priori reason to expect such contributions to be small, but little is known of those couplings. Including such contributions would add too many unknown parameters to the model.

F. Form factors

In this calculation, the prescription of assigning an overall form factor to gauge invariant sets of diagrams is adopted. This means, for instance, that all of the diagrams of the type shown in Fig. 1 have the same form factor as a multiplicative factor. For all of the form factors, the form

$$F = \left(\frac{X^4}{\left(p_i^2 - m_i^2\right)^2 + X^4} \right)^n \qquad (15)$$

is chosen.

In this expression, p_i is usually the momentum of the off-shell particle with mass m_i. In this calculation, the simplification of setting all of the p_i^2 to be equal to s, the total energy in the c.m. frame, squared, is made. X is chosen to be 1.8 GeV, as has been used by other authors. In addition, since this form factor is applied to sets of diagrams, m_i is chosen to be the mass of the lightest off-shell particle in a particular set. The exception to this occurs in the diagrams of Figs. 2(d) and 2(f), where m_i is chosen to be the mass of the vector meson in the diagram. The value of the integer n depends on the spin of baryons in the diagram. If there are only spin-1/2 baryons in the set of diagrams, n is chosen to be unity, while for spin-3/2 baryons, n is chosen to be 2.

IV. RESULTS

The polarization observables for this process are fivefold differential, which means that there are a number of different ways in which they can be displayed. Since it is not obvious how to display fivefold differential quantities, it is usual to integrate over some of the independent variables. In the following subsections, some of the kinematic variables are integrated over, showing the resulting observables as curves for different values of Φ^*.

Since the observables are either even or odd under the transformation $\Phi^* \leftrightarrow 2\pi - \Phi^*$, this variable is not integrated. Here Φ^* is the azimuthal angle that the plane containing the two kaons makes with the "reaction" plane, or the plane containing the momenta of the target and recoil nucleon, and the photon. Thus, in all the plots that follow, the observables are shown for four values of Φ^*: $\pi/6$, $\pi/4$, $\pi/3$, and $\pi/2$. Note that observables that are even in the Φ^* transformation could be displayed as Dalitz plots.

A. Presentation

Figure 4 shows the observable $P_x^{\odot}$ (the asymmetry that arises from circularly polarized photons incident upon nucleons polarized along the x axis), displayed as functions of four different variables. This means that all other independent variables have been integrated out. In each case, the curves are shown for four different values of Φ^*, as described above. For the curves in Fig. 4(a), the independent variable is $m_{K\overline{K}}$ [in all that follows, $m_{ab}^2 \equiv (p_a + p_b)^2$, where m_a is the mass
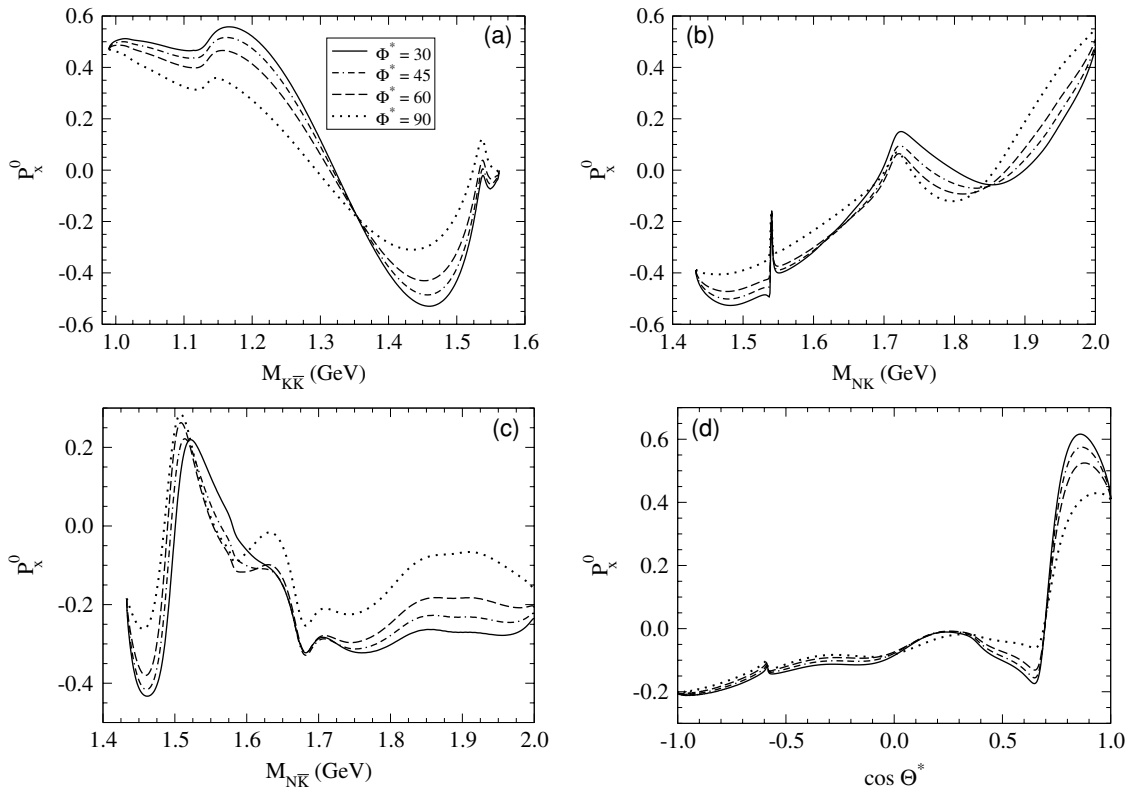

FIG. 4. The observable $P_x^{\odot}$ shown in terms of different kinematic variables. (a) as a function of $m_{K\overline{K}}$; (b) as a function of m_{NK}; (c) as a function of $m_{N\overline{K}}$; (d) as a function of $\cos \Theta^*$.
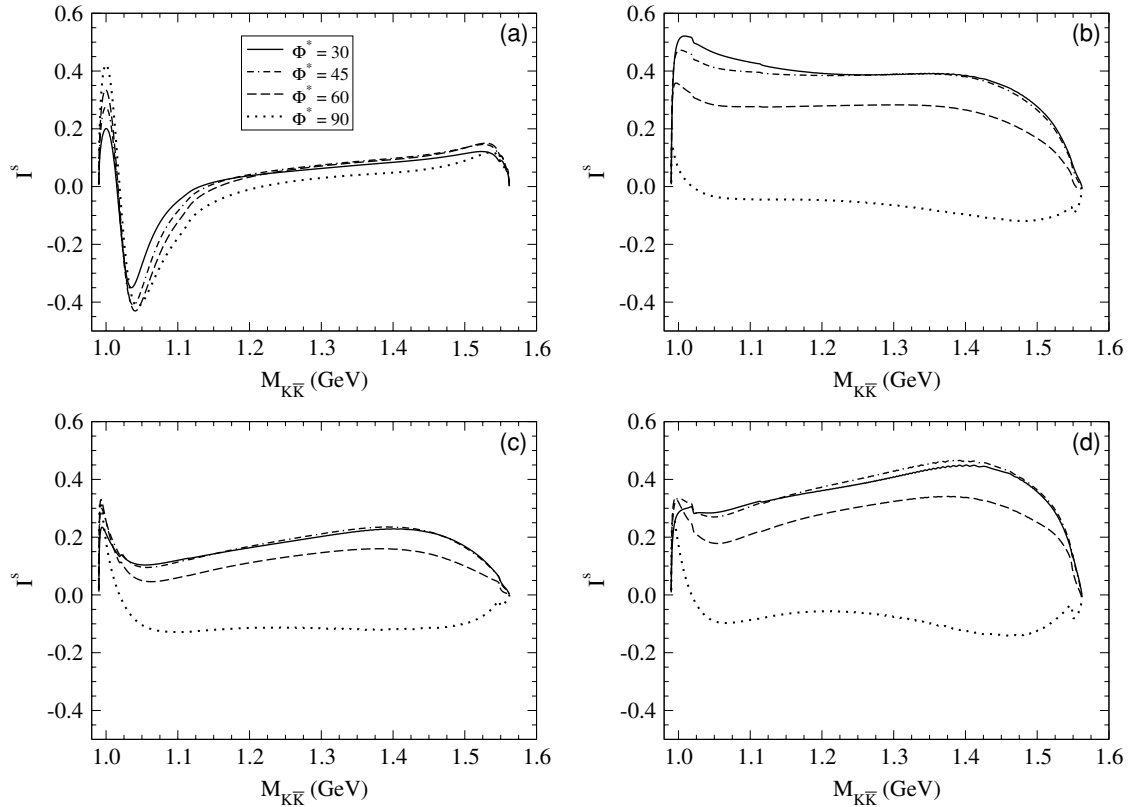
FIG. 5. The observable I^s, showing its sensitivity to the coupling constants G_v^ϕ and G_t^ϕ. (a) $G_v^\phi = 4$, $G_t^\phi = 0$; (b) $G_v^\phi = -4$, $G_t^\phi = 0$; (c) $G_v^\phi = 0$, $G_t^\phi = 4$; (d) $G_v^\phi = 0$, $G_t^\phi = -4$. In each case, the observable is shown as a function of $m_{K\overline{K}}$.

of particle a, and p_a is its four-momentum]. In the plot in Fig. 4(b), the independent variable is m_{NK}. In Fig. 4(c), it is $m_{N\overline{K}}$, while for Fig. 4(d), it is $\cos \Theta^*$. Θ^* is the polar angle of the $K\overline{K}$ pair in their rest frame, measured relative to the motion of the recoil nucleon. In these four plots, the content of the model is exactly the same (the process is $\gamma p \rightarrow n K^+ \overline{K}^0$), but the appearance of the observable is very different in each case. Note the effects of the $\Lambda(1520)$ near its resonant mass of 1.52 GeV in the curves in Fig. 4(c). Similarly, the effect of the Θ^+ is seen near its mass of 1.54 GeV in the curves in Fig. 4(b).

In Figs. 4(b) and 4(c), it might be more useful to use a different definition of Φ^*, one appropriate to the pair of hadrons whose invariant mass is treated as the independent variable. Thus, in Fig. 4(b), instead of Φ^* for the $K\overline{K}$ system (as defined earlier), it might be more appropriate to use Φ^*_{NK}, while for Fig. 4(c) $\Phi^*_{N\overline{K}}$ might be more appropriate. The reason is that if there is a resonance in the $K\overline{K}$ system, its decay products will yield a $\Phi^*_{N\overline{K}}$ distribution that characterizes the decay. In the same manner, a resonance in the NK ($N\overline{K}$) system should yield a Φ^*_{NK} ($\Phi^*_{N\overline{K}}$) distribution characteristic of its decay to NK ($N\overline{K}$).

B. Φ coupling constants

The two coupling constants G_v^ϕ and G_t^ϕ of Eq. (4) are not well known. A range of values has been explored in the literature. For example, in Ref. [10], the values explored for

G_v^ϕ were ± 3.0 and 1.0, with a preference for $G_v^\phi = +3.0$, with $\kappa_\phi (\equiv G_t^\phi / G_v^\phi) = 0.3$. Nakayama and Tsushima [11] explore a range of values between 0.0 and -2.0 for G_v^ϕ, with κ_ϕ taking the values 0.0, ± 0.5, and -4.0. In a later article [12], these authors use $G_v^\phi = -0.65$ with $\kappa_\phi = 0$, based on SU(3) and Okubo-Zweig-Iizuka (OZI) [13] arguments. These values are consistent with those used by Oh *et al.* [14], who set both coupling constants to zero, based on the simplest interpretation of the OZI rule [13]. Nakayama *et al.* [15] explore the values $G_v^\phi = -0.45$, -0.19, -0.90, and -0.40, with $\kappa_\phi = \pm 0.5$. Titov *et al.* [16] use $\kappa_\phi = 0$, with $G_v^\phi = -0.67$.

The discussion above indicates that it would be interesting to explore the effects that different choices for these coupling constants will have on a few of the polarization observables. Figures 5 and 6 show the effects on the observables I^s (Fig. 5) and $P_x^\odot$ (Fig. 6) of choosing different values for these constants. In each of these two figures, panel (a) corresponds to the choice $G_v^\phi = 4$, $G_t^\phi = 0$; panel (b) corresponds to $G_v^\phi = -4$, $G_t^\phi = 0$; panel (c) corresponds to $G_v^\phi = 0$, $G_t^\phi = 4$; and panel (d) corresponds to $G_v^\phi = 0$, $G_t^\phi = -4$. The process is $\gamma p \rightarrow p K^0 \overline{K}^0$. The values chosen are not completely inconsistent with the ranges discussed in the previous paragraph.

These four choices for the coupling constants lead to differential cross sections that are similar but not identical. In all of the figures, the effects of the ϕ show up most clearly near its resonant mass of 1.02 MeV (the independent variable in these plots is $m_{K\overline{K}}$), but the effects are also seen far away
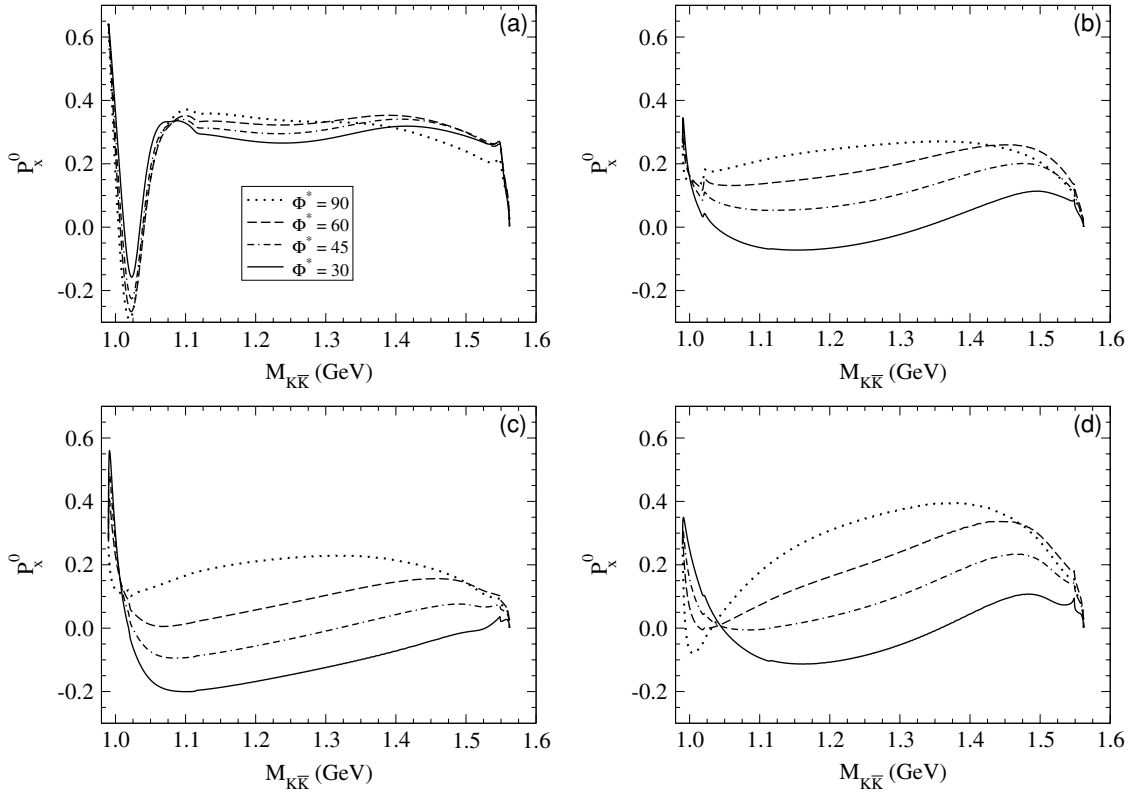
FIG. 6. The observable $P_x^\odot$, showing its sensitivity to the coupling constants G_v^ϕ and G_t^ϕ. (a) $G_v^\phi = 4$, $G_t^\phi = 0$; (b) $G_v^\phi = -4$, $G_t^\phi = 0$; (c) $G_v^\phi = 0$, $G_t^\phi = 4$; (d) $G_v^\phi = 0$, $G_t^\phi = -4$. In each case, the observable is shown as a function of $m_{K\overline{K}}$.

from this resonant mass. The changes that arise in simply changing the sign of G_v^ϕ [Figs. 5 and 6, panels (a) and (b)] are quite striking, as are the changes that arise when the coupling is changed from vector to tensor [panels (a) and (c) in each figure, for instance, and to a lesser extent, panels (b) and (d)]. One can argue that the inclusion of other $K\overline{K}$ resonances in the calculation will modify these effects. No doubt they will, but these observables will nevertheless be sensitive to the values and signs of the coupling constants of the ϕ. This means that polarization observables can be used to help pin down coupling constants such as the ones explored here.

C. Subthreshold resonance

The $\Lambda(1405)$ resonance is one of the relatively well-established hyperons. It lies just below the NK threshold, so its coupling (to NK) is not very well known. In the model used, the sensitivity to this state is explored by the display of a few observables with this state included in the calculation and the same observables with the state excluded. The effect of changing the coupling constant of this state is also explored. The observables examined are P_x^s (Fig. 7), I^c (Fig. 8), P_y^c (Fig. 9), and $\mathcal{O}_{yz'}^c$ (Fig. 10), in the process $\gamma p \rightarrow nK^+\overline{K}^0$. In each of these figures, the results when the $\Lambda(1405)$ is excluded are shown in the top panel. The middle panel shows the results obtained when this state is included, and the coupling constant $g_{\Lambda(1405)NK}$ is set to the value 5.3. The lowest panel corresponds to increasing this coupling constant to 8.0.

In all of these figures, the curves with the $\Lambda(1405)$ included are very different from those without it, especially near the

lowest values of $m_{N\overline{K}}$. For instance, in Fig. 7, the observable is near zero at threshold if the $\Lambda(1405)$ is excluded from the calculation, and becomes near -0.2 when it is included. In the case of Fig. 8 the observable goes from 0.0 to near 0.4, in the vicinity of the $N\overline{K}$ threshold, without and with the $\Lambda(1405)$, respectively. Similar effects are seen in Figs. 9 and 10. Changing the value of the coupling constant from 5.3 to 8.0 also induces noticeable (and, in some cases, significant) changes in the shapes of the observables near the $N\overline{K}$ threshold. Note that the effects of the state can be seen fairly far away from threshold, especially in Fig. 7. In this figure, at values of $m_{K\overline{K}}$ as large as 1.6 GeV [about 200 MeV away from the nominal mass of the $\Lambda(1405)$, whose total width is of the order of 50 MeV], the observable is small and positive when the $\Lambda(1405)$ is excluded from the calculation and becomes small and negative when the state is included. It can also be seen that as the coupling constant is increased, the shapes of the observables change. For instance, the value of P_x^s near the $N\overline{K}$ threshold (Fig. 7) changes from about -0.25 to -0.15 as $g_{\Lambda(1405)NK}$ changes from 5.3 to 8.0. In addition, in the same figure, the maximum at $m_{N\overline{K}} = 1.5$ GeV changes from 0.05 to 0.13 at $\Phi^* = 90°$. The change in the maximum near $m_{N\overline{K}} = 1.5$ in Fig. 10 is more striking, going from about 0.6 when $g_{\Lambda(1405)NK} = 5.3$ to 0.3 when $g_{\Lambda(1405)NK} = 8.0$, at $\Phi^* = 30°$. These features serve to illustrate that, in calculations such as this, "small" contributions may not affect the cross section much, but can have significant effects on polarization observables, even in regions where one might expect their effects to be small.
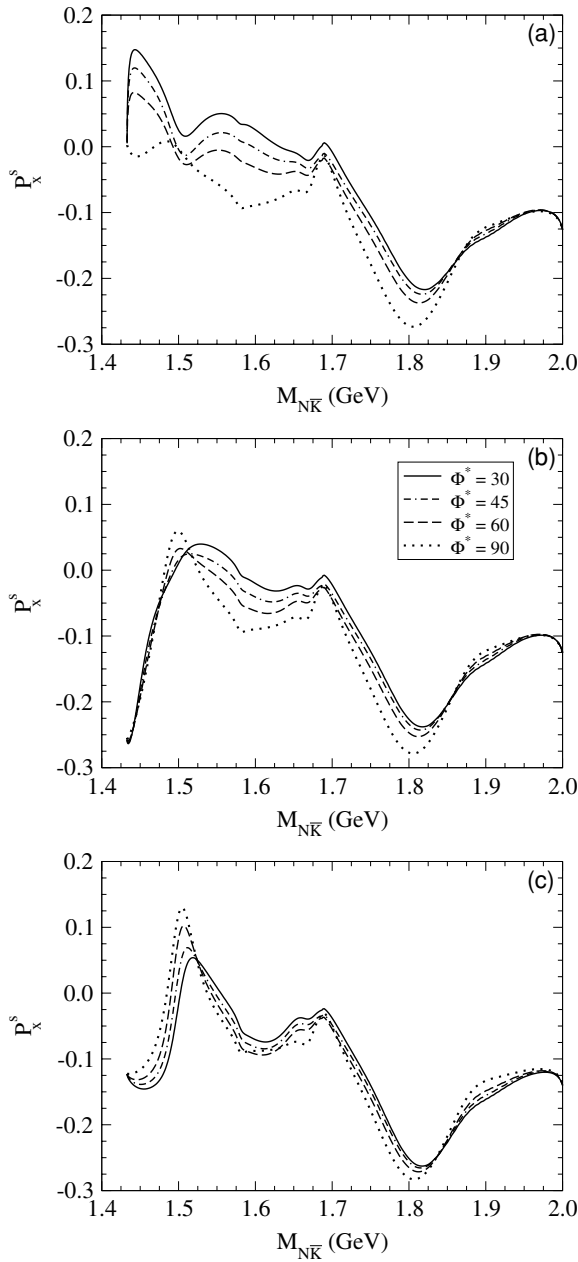
FIG. 7. The observable P_x^s, showing its sensitivity to the sub-threshold resonance $\Lambda(1405)$: (a) results with the $\Lambda(1405)$ excluded in the calculation; (b) results when this state is included, with $g_{\Lambda(1405)NK} = 5.3$; and (c) results when the coupling constant is increased from 5.3 to 8.0. All curves are shown as functions of $m_{N\overline{K}}$.

FIG. 8. The observable I^c, showing its sensitivity to the sub-threshold resonance $\Lambda(1405)$; (a) results with the $\Lambda(1405)$ excluded in the calculation; (b) results when this state is included, with $g_{\Lambda(1405)NK} = 5.3$, and (c) results when the coupling constant is increased from 5.3 to 8.0. All curves are shown as functions of $m_{N\overline{K}}$.

D. Pentaquark search

One very interesting question regarding these observables is their possible sensitivity to exotic resonances, such as the Θ^+ [17]. If observables are found that show sensitivity to this state, they can be used to confirm its existence (or otherwise), assuming production mechanisms like those presented in [3]. One of the disadvantages of using the differential cross section to search for states like this is that one state (or a few states) may provide a very large background against which a small signal must be sought. In the case of the pentaquark searches,
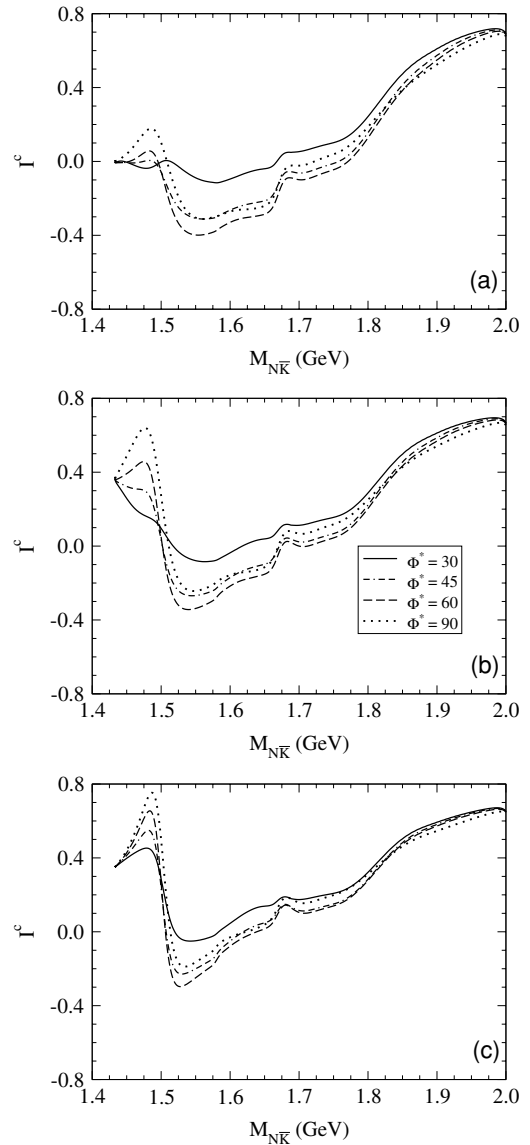
the large backgrounds are provided by the $\Lambda(1520)$, along with other nonexotic hyperons, as well as mesons like the ϕ. With polarization observables, large "backgrounds" are not necessarily a problem, and the curves that are shown illustrate what might be possible in pentaquark (or similar) searches.

In the model used for these calculations, the production cross section for the Θ^+ is of the order of a few nanobarns, consistent with the upper limit recently announced by researchers at JLab [5]. In the calculation, this size of cross section assumes that the pentaquark has $J^P = 1/2^+$, and that mechanisms involving the K^* are not important. In the same framework, the cross section obtained is significantly smaller if the state has $J^P = 1/2^-$. In either case, the cross sections for producing the nonexotic hyperons, particularly the $\Lambda(1520)$,
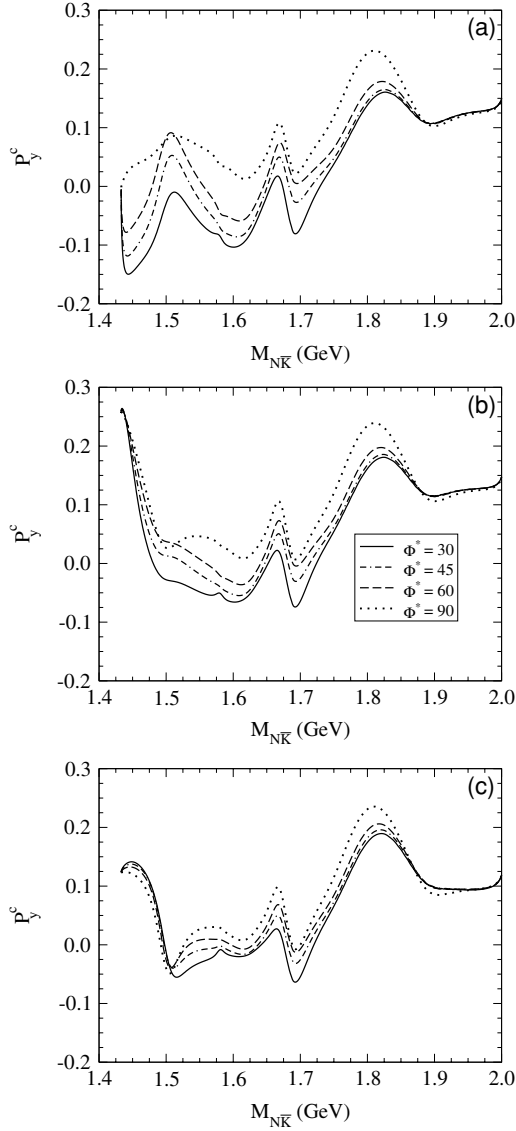
FIG. 9. The observable P_y^c, showing its sensitivity to the subthreshold resonance $\Lambda(1405)$: (a) results with the $\Lambda(1405)$ excluded in the calculation; (b) results when this state is included, with $g_{\Lambda(1405)NK} = 5.3$; and (c) results when the coupling constant is increased from 5.3 to 8.0. All curves are shown as functions of $m_{N\overline{K}}$.

FIG. 10. The observable $\mathcal{O}_{yz'}^c$, showing its sensitivity to the subthreshold resonance $\Lambda(1405)$: (a) results with the $\Lambda(1405)$ excluded in the calculation; (b) results when this state is included, with $g_{\Lambda(1405)NK} = 5.3$; and (c) results when the coupling constant is increased from 5.3 to 8.0. All curves are shown as functions of $m_{N\overline{K}}$.

are several hundred times larger, and would contribute to the difficulty of extracting a Θ^+ signal, if the state were to exist.

Figures 11–13 ($I^\odot$, $P_x^\odot$ and $P_z^\odot$, respectively) show the curves that result when there is no Θ^+ in the calculation [the curves in panel (a)], when a Θ^+ with $J^P = 1/2^+$ is included [the curves in panel (b)], and when a Θ^+ with $J^p = 1/2^-$ is included [the curves in panel (c)]. The process is $\gamma p \rightarrow n K^+ \overline{K}^0$. In Fig. 11, the helicity asymmetry without the pentaquark is small, but recent work has demonstrated that even such a small observable is measurable with high precision at JLab [2]. When the pentaquark is included in the calculation, this observable remains small, except for a structure in the region of the invariant mass of the pentaquark.

For a pentaquark of positive parity, the signal is significant, but extraction could still be a challenge, as the width of the
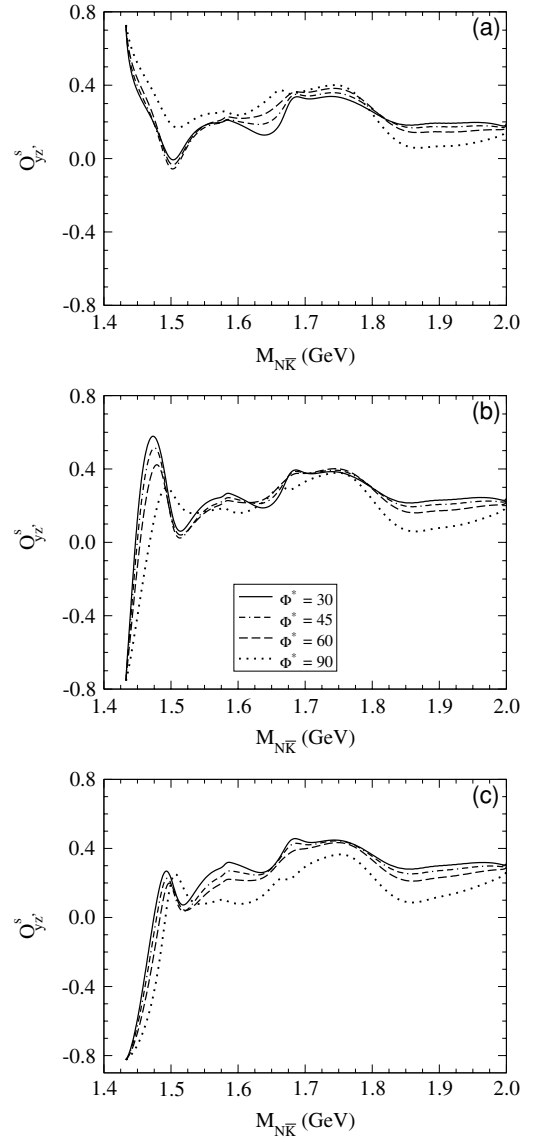
"structure" is similar to the width of pentaquark (here, a width of 1 MeV is used). For a pentaquark with negative parity, the theoretical curves also show a significant structure, but it is somwehat less so than for the case of a positive-parity pentaquark. One striking feature here is the difference in the "sign" of the signal between the positive- and negative-parity cases, suggesting that this observable could act as an excellent parity filter for the pentaquark. Note that this asymmetry has already been measured at JLab for $\gamma p \rightarrow p\pi^+\pi^-$ [2]. Thus it may be possible to measure it for $\gamma N \rightarrow N K\overline{K}$ relatively quickly.

Figures 12 and 13 show similar structures in the curves for $P_x^\odot$ and $P_z^\odot$, respectively. Note that, in all cases, the
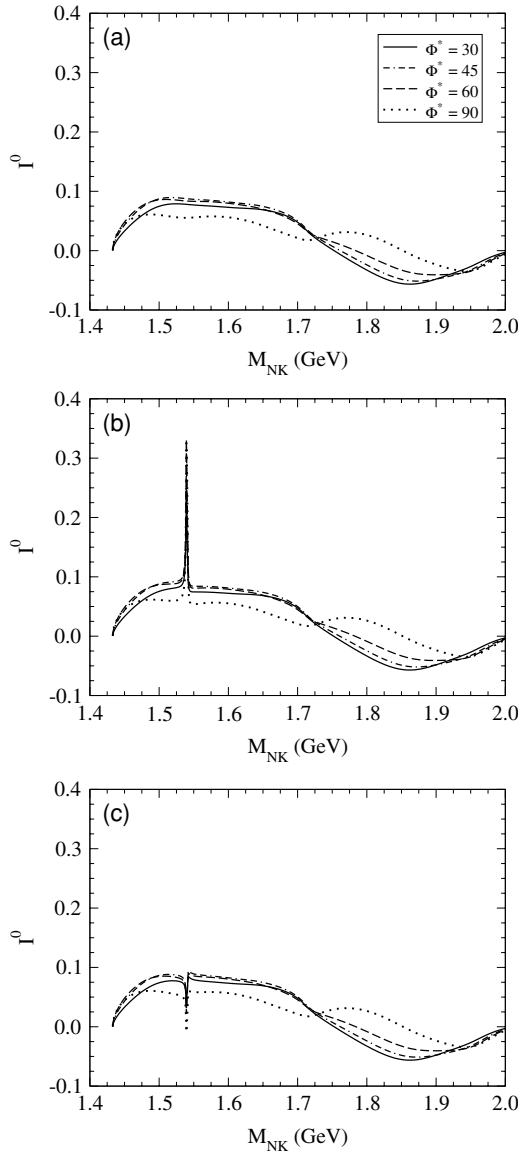
FIG. 11. The beam asymmetry $I^{\odot}$, showing its sensitivity to the exotic resonance Θ^{+}: (a) results when the Θ^{+} is excluded from the calculation, (b) results when a Θ^{+} of positive parity is included in the calculation, and (c) results when a Θ^{+} of negative parity is included in the calculation. All curves are shown as functions of m_{NK}.

FIG. 12. The observable $P_{x}^{\odot}$, showing its sensitivity to the exotic resonance Θ^{+}: (a) results when the Θ^{+} is excluded from the calculation, (b) results when a Θ^{+} of positive parity is included in the calculation, and (c) results when a Θ^{+} of negative parity is included in the calculation. All curves are shown as functions of m_{NK}.

structures stand out clearly for two reasons. The first is that the pentaquark is a narrow state, and the "width" of any structure that might be observed will be similar to that of the state giving rise to the structure. The second reason is that the Θ^{+} is the *only* resonance in the nK^{+} channel. All other resonances are in the $n\overline{K}^{0}$ channel. The kinematic reflections from these resonances will show up, as can be seen in Figs. 12 and 13, but the presence of the Θ^{+} in this channel has a marked effect. Note that in Fig. 13, this observable is predicted to be large (in the framework of the model used) and negative. A number of other observables utilizing linearly polarized photons (not shown here) show similar structures for the pentaquark. Note, too, that Oh, Nakayama, and Lee [14] show similar structures arising from the pentaquark (even though the "background"
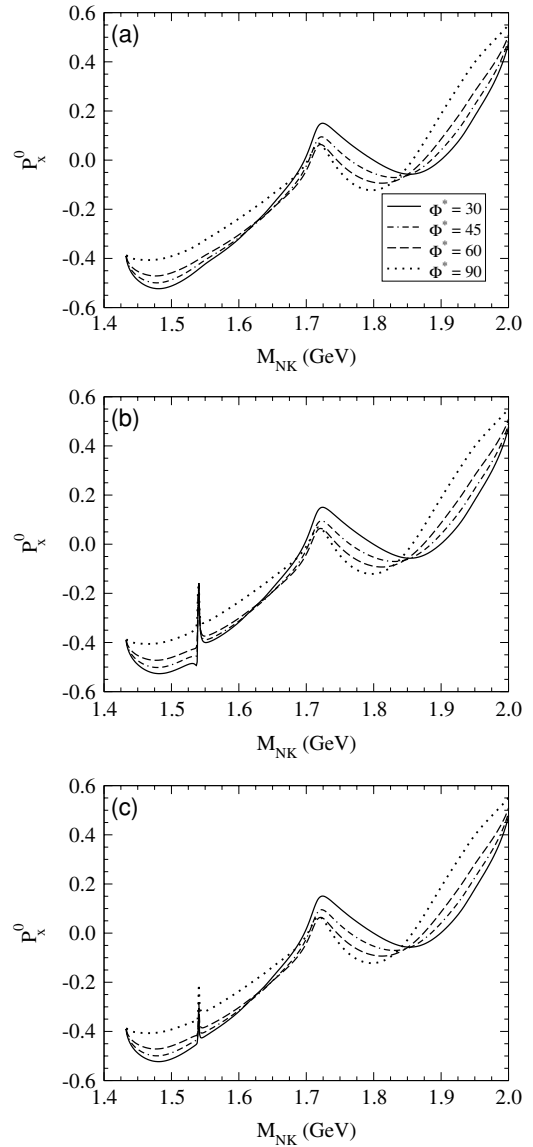
contributions appear completely different) for the process $\gamma n \rightarrow nK^{+}K^{-}$, for the observables they denote Σ_{x} ($\equiv I^{s}$ in the notation used herein) and C_{BT} ($\equiv P_{z}^{\odot}$). In addition, Nakayama and Tsushima [12] explore Σ_{x} in $\gamma n \rightarrow nK^{+}K^{-}$, but display their results as a function of one of the angles, rather than as a function of m_{NK}. It is therefore more difficult to compare their results with those presented herein.

It must be emphasized here that the potential signals shown above arise in the full model, including the contribution of the $\Lambda(1520)$. In the model, the cross section for production of this state is several hundred times larger than the cross section for producing the pentaquark. Despite this "inconvenient" ratio of production cross sections, the polarization observables explored above give clear signals for the pentaquark, and
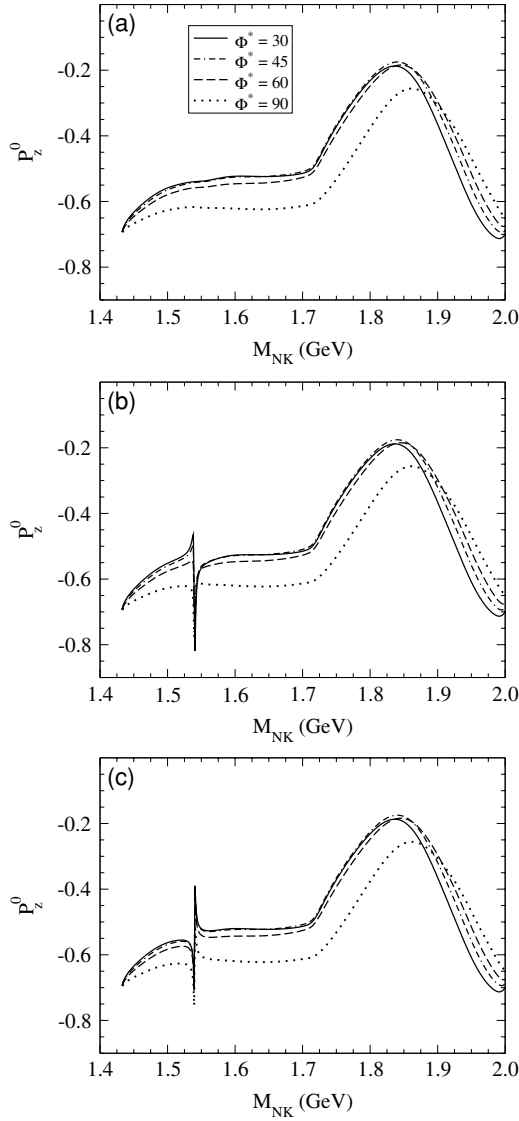
FIG. 13. The observable $P_z^{\odot}$, showing its sensitivity to the exotic resonance Θ^+: (a) results when the Θ^+ is excluded from the calculation, (b) results when a Θ^+ of positive parity is included in the calculation, and (c) results when a Θ^+ of negative parity is included in the calculation. All curves are shown as functions of m_{NK}.

FIG. 14. The observables (a) $I^{\odot}$, (b) $P_x^{\odot}$, and (c)$P_z^{\odot}$, showing their sensitivities to both the exotic resonance Θ^+ (with positive parity) and the nonexotic $\Lambda(1405)$. The solid curves all correspond to $\Phi^* = \pi/6$, while the dash-dotted curves are for $\Phi^* = \pi/2$. In each panel, the uppermost curves arise when the contibution of the $\Lambda(1405)$ is turned off. The lowermost curves result when $g_{\Lambda(1405)NK} = 8.0$, while the middle curves arise when this coupling constant has a value of 5.3. All curves are shown as functions of m_{NK}.

extraction of these signals will depend mainly on the energy resolution possible in any experiment and much less so on the necessity of extracting a small signal from a large background. It must also be noted that the "heights" of the signals shown for the pentaquark are independent of its width: only the width of the signals reflects the width of the pentaquark.

One question of interest for these signals is the robustness of the predictions with regard to other details in the model. There are many parameters that may be varied to get some idea of the model dependence in the "pentaquark signals." Here, their dependence on the coupling constant $g_{\Lambda(1405)NK}$, discussed in the previous subsection, is displayed. Figure 14 shows curves for (a) $I^{\odot}$; (b) $P_x^{\odot}$, and (c) $P_z^{\odot}$, for $\Phi^* = 30°$ (solid curves) and $\Phi^* = 90°$ (dash-dotted curves). Each panel shows curves for three values of $g_{\Lambda(1405)NK}$, namely 0, 5.3 and 8.0, as indicated
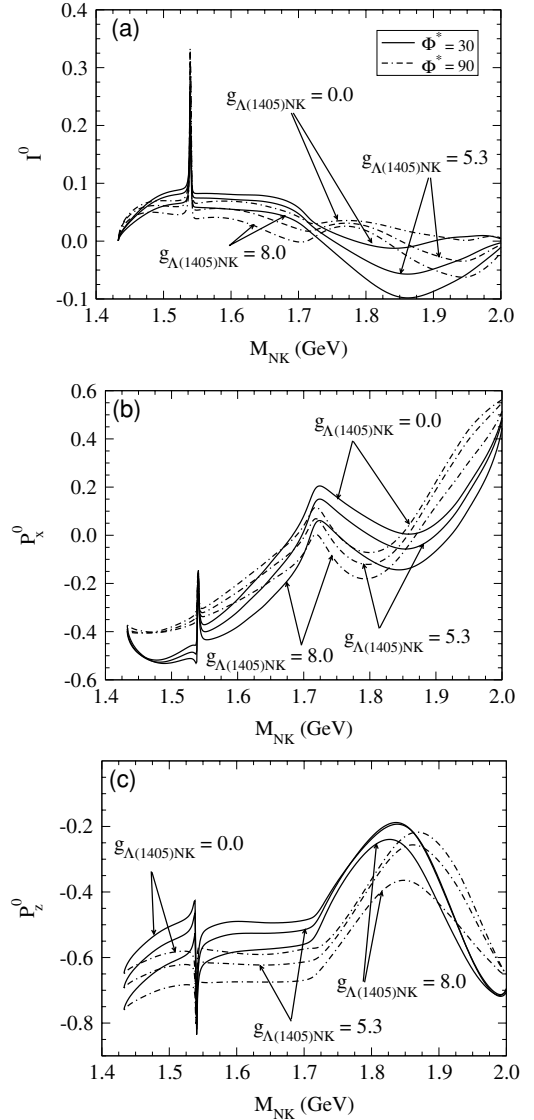
on the graphs. From these graphs, it can be concluded that the strength of the pentaquark signal is independent of the value of the coupling constant $g_{\Lambda(1405)NK}$, especially for $I^{\odot}$, shown in Fig. 14(a).

In the above, three observables have been chosen to illustrate how it might be possible to use these polarization observables in pentaquark searches. The three observables chosen all required circularly polarized photons. It must be noted here that all 63 observables show some kind of effect that is due to the pentaquark, and some of the effects are quite striking. With the cross section for production of the Θ^+ being of the order of a few nanobarns or smaller, it becomes crucial

that observables such as the ones discussed here be exploited to provide other means of finding or refuting this state.

V. CONCLUSION AND OUTLOOK

The results presented above were obtained in the context of a particular model, and, as such, they are clearly model dependent. Nevertheless, within the framework of *this particular model*, there has been some attempt to show how useful these polarization observables can be by exploring their sensitivity to a few details of the model. Comments on what other models would predict for such observables cannot be made at this time. In the case of the signals shown for the pentaquark, it would be unwise to speculate on the nature of such signals in other models. It must be emphasized that the discussion and plots shown are only indications of what information these observables may be able to convey. Any useful information to be gleaned from measurements of such observables must be extracted with full analyses. The model used to illustrate what is possible should not be construed as providing the "final word" on these observables.

A number of points about the polarization observables developed in [1] have been conveyed. The first point is that these observables may be displayed in a number of ways. The second, and perhaps most obvious, point to note is that, however they are displayed, these observables exhibit an enormously rich structure, reflecting the degree of complexity in the underlying dynamics. This sensitivity to the various

contributions leading to the final state being studied, especially to "small" contributions, provides an indispensible tool that will need to be fully exploited in attempts to understand processes like the ones discussed herein. Such processes are expected to be among the primary sources of information in the ongoing attempts to understand the dynamics of soft QCD.

As has been mentioned before, a number of these observables should be accessible in the near future at existing facilities, in a number of different processes. The obvious applications are to the process discussed herein, $\gamma N \to N K \overline{K}$, and to $\gamma N \to N \pi \pi$. However, final states like $N \eta \pi$, $N \eta \eta$, $Y K \pi$ (where Y is a Λ or Σ), $Y K \eta$, and even $K K \Xi$, will require the same kinds of measurements in order to disentangle the various contributions leading to them. In the processes that produce hyperons in the final states, their various self-analyzing decays provide access to recoil polarization measurements, thus opening up more possibilities. Many of these opportunities will have to be seized for continued progress to be made in the understanding of baryon spectroscopy.

[1] W. Roberts and T. Oed, Phys. Rev. C **71**, 055201 (2005).

[2] S. Strauch (CLAS Collaboration), J. Phys. Conf. Ser. **9**, 268 (2005); S. Strauch (CLAS Collaboration), in *Proceedings of the Second Conference on Nuclear and Particle Physics with CEBAF at JLab (NAPP 2003) Dubrovnik, Croatia, 26–31 May 2003*, submitted to Fizika B; S. Strauch *et al*. (CLAS Collaboration), Phys. Rev. Lett. **95**, 162003 (2005).

[3] W. Roberts, Phys. Rev. C **70**, 065201 (2004).

[4] J. Barth *et al*. (SAPHIR Collaboration), Phys. Lett. **B572**, 127 (2003); V. Kubarovsky *et al*. (CLAS Collaboration), Phys. Rev. Lett. **92**, 032001 (2004) [Erratum-*ibid*. **92**, 049902 (2004)].

[5] V. D. Burkert, arXiv:hep-ph/0510309, invited talk at the 22nd International Symposium on Lepton-Photon Interactions at High Energy (LP 2005), Uppsala, Sweden, 30 Jun–5 Jul. 2005 and invited talk at the 6th European Research Conference on Electromagnetic Interactions with Nucleons and Nuclei (EINN 2005), Milos Island, Greece, 19–24 Sep. 2005 and invited talk at International Workshop on the Physics of Excited Baryons (NSTAR 05), Tallahassee, Florida, 10–15 Oct. 2005; M. Battaglieri, *et al*. (CLAS Collaboration), submitted to Phys. Rev. Lett.

[6] S. Eidelman *et al*., Phys. Lett. **B592**, 1 (2004).

[7] S. Nussinov, hep-ph/0307357; R. A. Arndt, I. I. Strakovsky, R. L. Workman, Phys. Rev. C **68**, 042201(R)(2003) [Erratum, **69**, 019901 (2004)]; J. Haidenbauer and G. Krein, *ibid* **68**, 052201(R) (2003); R. Cahn and G. Trilling, Phys. Rev. D **69**, 011501(R) (2004); A. Sibirtsev, J. Haidenbauer, S. Krewald, and

U. G. Meissner, Eur. Phys. J. A **23**, 491 (2005); Phys. Lett. **B599**, 230 (2004); W. R. Gibbs, Phys. Rev. C **70**, 045208 (2004).

[8] S. I. Nam, A. Hosaka, and H.-Ch. Kim, Phys. Lett. **B579**, 43 (2004); hep-ph/0403009, submitted to Phys. Rev. D.

[9] Y. Oh, H. Kim, and S. H. Lee, Phys. Rev. D **69**, 074016 (2004); **69**, 014009 (2004); Nucl. Phys. **A745**, 129 (2004).

[10] K. McCormick *et al*. (CLAS Collaboration), Phys. Rev. C **69**, 032203 (2004).

[11] K. Tsushima and K. Nakayama, Phys. Rev. C **68**, 034612 (2003).

[12] K. Nakayama and K. Tsushima, Phys. Lett. **B583**, 269 (2004).

[13] S. Okubo, Phys. Lett. **B5**, 165 (1963); G. Zweig, CERN report no. 8419/ TH 412 (1964); I. Iizuka, Prog. Theor. Phys. Suppl. **37/38**, 21 (1966).

[14] Y. Oh, K. Nakayama, and T. S. Lee, Phys. Rep. **423**, 49 (2006).

[15] K. Nakayama, J. W. Durso, J. Haidenbauer, C. Hanhart, and J. Speth, Phys. Rev. C **60**, 055209 (1999).

[16] A. I. Titov, B. Kampfer, and B. L. Reznik, Phys. Rev. C **65**, 065202 (2002).

[17] T. Nakano *et al*. (LEPS Collaboration), Phys. Rev. Lett. **91**, 012002 (2003); V. Barmin *et al*. (DIANA Collaboration), Phys. At. Nucl. **66**, 1715 (2003) [Yad. Fiz. **66**, 1763 (2003)]; S. Stepanyan *et al*. (CLAS Collaboration), Phys. Rev. Lett. **91**, 252001 (2003); A. E. Asratyan, A. G. Dolgolenko, and M. A. Kubantsev, Phys. At. Nucl. **67**, 682 (2004) [Yad. Fiz. **67**, 704 (2004)]; A. Airapetian *et al*. (HERMES Collaboration), Phys. Lett. **B585**, 213 (2004); A. Aleev *et al*. (SVD Collaboration), hep-ex/0401024, submitted to Yad. Fiz.; M. Abdel-Bary *et al*. (COSY-TOF Collaboration), Phys. Lett. **B595**, 127 (2004).